## Design of fragile topological flat bands in an optical microcavity array

Yuhui Wang,\* Shupeng Xu<sup>®</sup>,\* Liang Feng<sup>®</sup>, and Ritesh Agarwal<sup>†</sup>
Department of Materials Science and Engineering, University of Pennsylvania,
and Philadelphia, Pennsylvania 19104, USA

(Received 27 February 2024; revised 29 May 2024; accepted 3 June 2024; published 1 July 2024)

Topological flat bands are increasingly recognized as an important paradigm to study the effects of quantum geometry and topology in strongly correlated systems. The recently discovered theory of fragile topology offers an alternative approach toward the understanding and realization of topological phases of matter. In Bosonic systems, though fragile topological phases have been experimentally realized, specific proposals of the experimental platform of topological flat bands have not been reported much. In this work, we introduce a photonic lattice obtained from coupled Kagome and triangular lattices designed based on the topological quantum chemistry theory, which supports topologically nontrivial flat bands. We further discuss the potential experimental realization in a microcavity array, as a platform that can be extended into the interacting regime through the formation of exciton-polaritons via coupling the optical modes to excitons. Notably, we show that the inevitable in-plane polarization splitting in optical microcavities will not hinder the construction of topological quasiflat bands. This work paves the way toward the experimental exploration of nontrivial topology in Bosonic flat bands, offering potential channels for its direct observation.

### DOI: 10.1103/PhysRevB.110.045401

#### I. INTRODUCTION

Dispersionless bands, i.e., flat bands, are commonly recognized as one of the key paradigms to study physical phenomena based on strong correlation and interactions due to the dominance of interaction energy U over the quenched kinetic energy. Additionally, nontrivial topology can be integrated with flat bands and thus induce novel phenomena, of which one significant example is topological flat bands (TFBs) superconductivity [1–7]. The significance of TFBs in superconductivity is supported by their connection to quantum metrics and contribution to superfluid weight or stiffness, which is not accessible in a trivial flat band. The nontrivial term in the superfluid weight was initially discussed in Chern flat bands [1], and has later been extended to flat bands with fragile topology [3]. Fragile topology is a topological phase that exhibits obstruction to constructing exponentially localized, symmetric Wannier functions (in short "'Wannier obstruction"), yet can be trivialized by the addition of appropriate trivial bands [8]. Wannier obstruction can be characterized by symmetry-based approaches [9–11]. Among these approaches, the topological quantum chemistry (TOC) theory offers a generalized, efficient approach to characterize and design topological bands [10-12] based on symmetry representations [13–15], of which the minimal building blocks are atomic limit bands, termed elementary band representations (EBRs).

Although in Fermionic systems, many theoretical and experimental attempts have been made to study TFB superconductivity, the extension of TFBs to Bosonic systems is less

explored. The study of the integration of topological nontriviality with flat band physics is still in a relatively early stage, especially in the Bosonic context [16] in spite of pioneering theoretical works [17,18] focusing on the excitation spectra of Bose-Einstein condensation (BEC) in trivial flat bands. It is intuitively expected that the topological nontriviality may induce novel phenomena in interacting Bosonic systems [19].

A following important question is, how can one design an experimentally accessible Bosonic lattice system with TFBs as the platform to further study TFBs in interacting Bosonic systems? To realize flat bands with nonzero Chern numbers generally entails complex coupling arrangements [20-23], strong magnetic field, and cryogenic temperature. Since the time-reversal symmetry of bosons is fundamentally distinct from that of Fermions, the topological  $\mathbb{Z}_2$  insulator is also not accessible. Consequently, TFBs designed based on specific crystalline symmetry naturally emerge as a viable option. Though some earlier reports have realized Bosonic fragile topological systems [24–26], studies related to realizing TFBs and the properties emerging from the interplay of quantum geometry and strong interactions have not been reported. Here, we propose an optical microcavity array that supports fragile TFBs based on the TQC theory, as an initial step to extend the study of TFBs to Bosonic systems, particularly compatible with many-body interactions. The main text is organized as follows: the general strategy of constructing fragile TFBs is reviewed and introduced based on the disconnected decomposable EBRs [12,27] via an explicit example of an s-orbital Hamiltonian. Next, the Hamiltonian is re-constructed with linearly polarized modes, as the electromagnetic proposition of the s-orbital model, where the physical consequence of in-plane polarization splitting is addressed. We demonstrate that the change in site symmetry and band representations will not destroy the topological properties of the flat bands. Lastly,

<sup>\*</sup>These authors contributed equally to this work.

<sup>†</sup>Contact author: riteshag@seas.upenn.edu

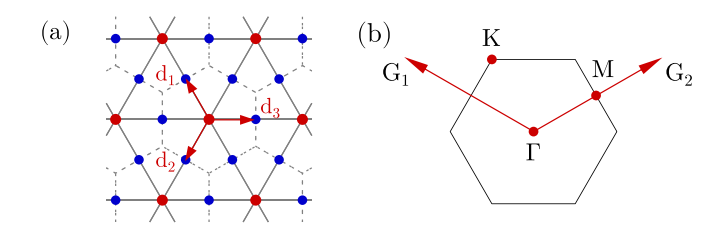


FIG. 1. (a) Wyckoff positions 1a (red dots at unit-cell centers) and 3c (blue dots at edge centers) in the space group p6mm.1', with site symmetry of point group (PG) 6mm and mm2, forming a triangular and Kagome lattice, respectively. (b) High symmetry points in the first Brillouin zone  $\Gamma$ , K, and M. Two reciprocal vectors are noted as  $G_1$  and  $G_2$ .

we discuss the potential experimental realization of fragile TFBs in an optical microcavity array with detailed numerical simulations.

### II. PRINCIPLE OF CONSTRUCTION OF FRAGILE TFBs

It has been realized from the previous work [24,28] that photonic crystals constructed based on the 3c Wyckoff position of the space group p6mm.1' [Fig. 1(a)] can potentially support the topological phase if the corresponding EBR is appropriately disconnected. In this case, at least one of the disconnected band representations is necessarily topologically nontrivial [8,12]. A specific case is when one of the two disconnected band representations is an EBR, then the other one exhibits fragile topology [8]. In the p6mm.1' case, with s-orbital states at 3c (point group mm2) Wyckoff positions represented by the irreducible representation (irrep)  $A_1$  (see the Supplemental Material for detailed descriptions [29]), the corresponding EBR can be written as

$$(A_1 \uparrow G)_{3c} = \{ \Gamma_1 \oplus \Gamma_5, K_1 \oplus K_3, M_1 \oplus M_3 \oplus M_4 \}$$
  
=  $\{ \Gamma_1, K_1, M_1 \} \oplus \{ \Gamma_5, K_3, M_3 \oplus M_4 \},$  (1)

where  $\Gamma$ , K, and M are high symmetry momenta marked in Fig. 1(b). Notice that  $\{\Gamma_1, K_1, M_1\}$  is an EBR and can be induced from s-orbital states at the 1a site (point group 6mm), represented by  $A_1$ . Hence, according to the previous deduction, the remaining two bands  $\{\Gamma_5, K_3, M_3 \oplus M_4\}$  are a set of fragile topological bands. In this Kagome lattice,  $(A_1 \uparrow G)_{1a}$  can be constructed as the synthetic s-orbital state formed by the equal-phase superposition of s-orbital states at 3c sites. Naturally, we can introduce another s-orbital state at the 1a site, corresponding to a triangular lattice [red sites in Fig. 1(a)], to only couple with the quasi-s-orbital state. This coupling setting can be realized by introducing identical real couplings only between 1a and the nearest neighboring 3c sites [solid arrows in Fig. 2(a)], preserving  $C_6$  symmetry. If all couplings are originally set to zero, the lattice is at its atomic limit, forming four (1+3) degenerate flat bands. After introducing these couplings between 1a and 3c sites, two complete band gaps will be formed across the entire BZ, and the residual two bands will stay degenerate and flat with the representation

$${A_1 \uparrow G}_{3c} \ominus {A_1 \uparrow G}_{1a} = {\Gamma_5, K_3, M_3 \oplus M_4}.$$
 (2)

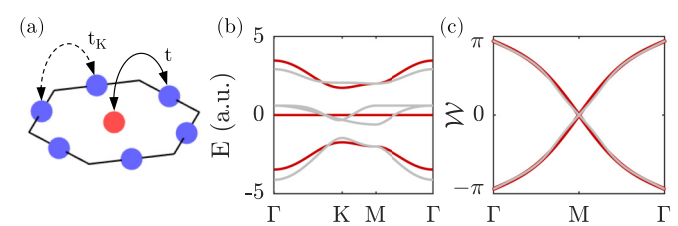


FIG. 2. Tight binding model of *s*-orbital states in  $A_1$  representation. (a) Schematic of the lattice, where t measures the coupling between 1a and 3c sites (solid arrows), and  $t_K$  for the Kagome lattice couplings (dashed arrows). (b) Calculated band diagram with t=-1.0,  $t_K=0$  (red) and  $t_K=-0.3$  (gray). Note that Kagome coupling renders the central two bands dispersive and nondegenerate. (c) Calculated Wilson loop spectra correspond to  $t_K=0$  (red) and  $t_K=-0.3$  (gray), both showing a winding feature.

Consequently, we construct two fragile topological flat bands based on the simple couplings between two lattices.

Subsequently, we explicitly write down the Hamiltonian. With two distinct on-site energies at 1a and 3c sites and the couplings among 3c (Kagome) sites included, the total tight-binding Hamiltonian as the sum of three parts is

$$\mathcal{H} = 2t \sum_{i=1}^{3} [a_{1a}^{\dagger} a_{3c,i} \cos(k_i) + \text{H.c.}], \quad \mathcal{H}_0 = U a_{1a}^{\dagger} a_{1a},$$

$$\mathcal{H}_{K} = 2t_{K} \sum_{\{i,j\}} [a_{3c,i}^{\dagger} a_{3c,j} \cos(k_{i} + k_{j}) + \text{H.c.}].$$
 (3)

Here,  $a_{1a,3c}$  are annihilation operators of orbital states of corresponding Wyckoff positions.  $\mathcal{H}$  is the Hamiltonian that captures the core idea of the construction of fragile TFBs that orbitals at the 1a site couple with orbitals at 3c sites with a real and constant coupling strength t.  $\mathcal{H}_0$  and  $\mathcal{H}_K$  address the effect of distinct onsite energy U at 1a sites and Kagome coupling between 3c and 3c sites given by  $t_K$ . In  $\mathcal{H}$  and  $\mathcal{H}_K$ ,  $k_i = k \cdot d_i$ , where  $d_1 = a[-1/2, \sqrt{3}/2]$ ,  $d_2 = a[-1/2, -\sqrt{3}/2]$ , and  $d_3 = a[1, 0]$ , and a is the distance between nearest neighboring sites [Fig. 1(a)]. H.c. corresponds to the Hermitian conjugate. Index pairs  $\{i, j\} = \{1, 2\}, \{1, 3\}, \{2, 3\}$  describe the nearest neighboring coupling between 3c sites.

The most simplified, ideal case is with U = 0 and  $t_K = 0$ , of which we only need to discuss  $\mathcal{H}$ . The corresponding band diagram is shown in red in Fig. 2(b), where two degenerate perfectly flat bands at zero energy can be observed. The physical picture is also nicely presented in the molecularorbital (MO) representations:  $\mathcal{H} = 2t(M_1^{\dagger}M_2 + \text{H.c.})$ , where the two molecular orbital operators are defined as  $M_1 = a_{1a}$ and  $M_2 = \sum_{i=1}^{3} a_{3c,i} \cos(k_i)$  [33,34]. The molecular orbital  $M_2$  here equivalently describes the synthetic s-orbital state. MO representation additionally elucidates that the rank of the Hamiltonian is two with four s-orbital states originally involved, determining the perfect degenerate band flatness. Also,  $\mathcal{H}_0 = U a_{1a}^{\dagger} a_{1a} = U M_1^{\dagger} M_1$  implies that the difference of on-site energy at 1a and 3c sites will not affect the band flatness. With a nonzero  $t_K$ , the central two bands are not strictly flat and degenerate [see gray bands in Fig. 2(b) with  $t_K = -0.3$ ]. However, the nontrivial fragile topology is preserved as long as the band representation of the central two bands is not altered by finite  $t_K$ . The bands will be connected

at  $t = t_K$  and as long as the magnitude of  $t_K$  is smaller than t, the current band representations [Eq. (2)] are valid. Another indicator of the topological nontriviality is the winding Wilson loop spectrum [35,36]. The geometry of the Wilson loop calculation is denoted in Fig. 1(b), where the closed loop is along the reciprocal lattice vector  $G_1$  and the spectra are plotted as the loop moves along  $G_2$  following the  $\Gamma$ -M- $\Gamma$  path. The spectrum of the calculated Wilson loop indicates a winding feature providing direct evidence that the central two bands of the proposed system are Wannier obstructed and hence topologically nontrivial [red in Fig. 2(c)]. Another calculated Wilson loop spectrum corresponds to the  $t_K = -0.3$  case shown in Fig. 2(b), confirming that weak Kagome coupling preserving the band representations will not trivialize the central two bands [gray in Fig. 2(c)].

# III. TIGHT-BINDING MODEL OF ELECTROMAGNETIC MODES

In order to explore the physical consequence of the topological nontriviality in a Bosonic system beyond the single particle picture, we specifically consider the electromagnetic (EM) realization in an optical microcavity array due to its compatibility to interacting Bosonic systems such as exciton-polaritons. Optical microcavities can also enable direct observation across both real and momentum space, including dispersion, excitation spectra, and phase coherence [37–40].

We first construct the model with two degenerate circularly polarized eigenmodes. Without any polarization splitting, these two eigenmodes will act similarly as two copies of sorbital Hamiltonians previously introduced. It should be noted that the mirror operation will then inverse the polarization mutually and  $C_2$  may add a  $\pi$  phase to the circularly polarized modes. Due to the finite longitudinal-transverse (LT) polarization splitting [41], originating from distinct boundary conditions for TE and TM modes in Maxwell equations, the degeneracy of these two copies of Hamiltonians is removed if not protected by symmetry. The site symmetry at 1a Wyckoff positions remains PG 6mm1' and we choose the irrep to be  $E_1$ since there is no symmetry breaking that breaks the degeneracy of two circularly polarized modes. The site-symmetry PG mm21' at 3c Wyckoff positions supports two independent and orthogonal linearly polarized states: one is parallel to edges of the unit cell and the other one is normal to edges, noted as azimuthal (A) and radial (R) modes and corresponding to  $B_1$  and  $B_2$  representations, respectively (see the Supplemental Material for a more detailed description of irreps [29]). Azimuthal and radial modes are represented in p-orbital-like features in Fig. 3(a), color coded in blue and red, respectively, to illustrate how they are aligned. We emphasize that no modes corresponding to higher orbital angular momentum numbers are involved in the current model.

The new induced band representations accounting for eigenmodes corresponding to different polarizations can be written as

$$(E_{1} \uparrow G)_{1a} = \{\Gamma_{6}, K_{3}, M_{3} \oplus M_{4}\},$$

$$(B_{1} \uparrow G)_{3c} = \{\Gamma_{3} \oplus \Gamma_{6}, K_{1} \oplus K_{3}, M_{1} \oplus M_{2} \oplus M_{3}\}, \quad (4)$$

$$(B_{2} \uparrow G)_{3c} = \{\Gamma_{4} \oplus \Gamma_{6}, K_{2} \oplus K_{3}, M_{1} \oplus M_{2} \oplus M_{4}\}.$$

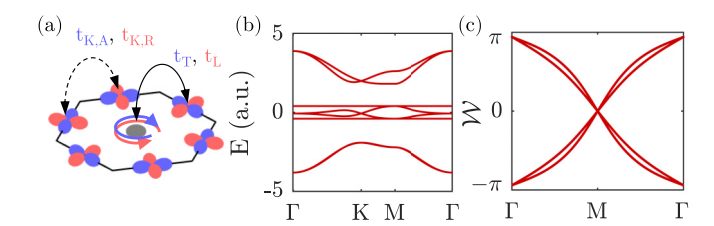


FIG. 3. Tight binding model of the EM-field realization of TFBs in  $E_1$ ,  $B_1$ , and  $B_2$  irreps. (a) Schematic of the lattice,  $t_T$  stands for the transverse coupling to the azimuthal modes (blue) and  $t_L$  stands for the longitudinal coupling to the radial modes (red).  $t_{K,A}$  stands for the couplings between the azimuthal modes at 3c Kagome sites, and  $t_{K,R}$  stands for the Kagome couplings between radial modes. (b) Calculated band diagram with  $t_L = -1.2$ ,  $t_T = -1$ ,  $t_A = -0.4$ ,  $t_R = 0.4$ , and  $t_R = 0.4$ , and

Similarly, we obtain the expected fragile topological band representation

$$(B_1 \uparrow G)_{3c} \oplus (B_2 \uparrow G)_{3c} \ominus (E_1 \uparrow G)_{1a}$$
  
=  $\{\Gamma_3 \oplus \Gamma_4 \oplus \Gamma_6, K_1 \oplus K_2 \oplus K_3, 2(M_1 \oplus M_2)\}, (5)$ 

which is not an EBR. Note that in Eq. (5), the  $C_2$  symmetry eigenvalues of corepresentations at  $\Gamma$ , namely,  $\Gamma_{3,4,6}$ , are -1 and those of corepresentations  $M_{1,2}$  are +1, respectively. This specific combination of symmetry eigenvalues cannot be found in any EBR in the p6mm.1' group, which confirms the topological nature of the bands. The main parameters in the corresponding Hamiltonian include on-site energy of two degenerate modes at the 1a site  $U_{1a}$  and on-site energy of azimuthal and radial modes at 3c sites  $U_A$  and  $U_R$ , respectively; The coupling between azimuthal and radial modes to 1a modes are noted as  $t_T$  and  $t_L$ , respectively. To account for the effect of Kagome couplings between 3c sites, we also introduce the Kagome couplings between azimuthal modes and radial modes to be  $t_{K,A}$  and  $t_{K,R}$ , respectively. Detailed Hamiltonian representing the EM field case is discussed in the Supplemental Material [29].

The band diagram calculated from this EM tight-binding model is shown in Fig. 3(b), with  $t_L = -1.2$ ,  $t_T = -1$ ,  $U_A = -0.4$ , and  $U_R = 0.4$ . We intentionally defined  $t_T \neq t_L$  and  $U_A \neq U_R$  so that the central four bands are not completely degenerate. In this case, two upper bands, four central bands, and two lower bands correspond to band representations  $(E_1 \uparrow G)_{1a}$ ,  $(B_1 \uparrow G)_{3c} \oplus (B_2 \uparrow G)_{3c} \oplus (E_1 \uparrow G)_{1a}$ , and  $(E_1 \uparrow G)_{1a}$ , respectively, as designed [Eq. (5)]. With zero Kagome coupling in the model, two perfectly flat bands can be observed in Fig. 3(b). The corresponding Wilson loop of the central four bands is demonstrated in Fig. 3(c), indicating two sets of winding branches in the Wilson spectra, degenerate at 0 and  $\pm \pi$  points.

## IV. ELECTROMAGNETIC NUMERICAL SIMULATIONS

To further examine the experimental accessibility and evaluate the performance of our theoretical model, we carried out 3D numerical simulations of the eigenfrequency spectrum of

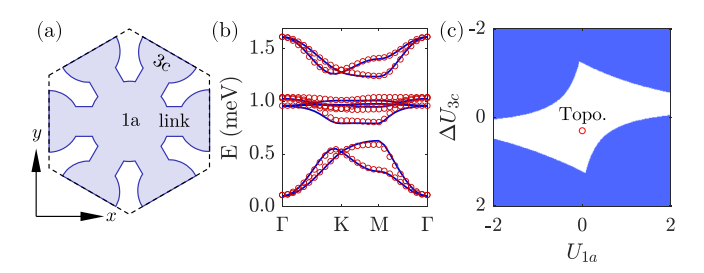


FIG. 4. (a) Schematic of the planar cavity lattice structure in numerical simulations. The cavity region corresponding to high refractive index are shaded. Cylindrical resonators at 1a and 3c sites are connected by links, while resonators at 3c sites are mutually separated. (b) Numerically simulated band diagram (marked in red circles) and tight binding fitting (plotted in blue lines). Complete gaps can be observed between central four bands and the other two sets of bands. A base energy of 1257 meV has been subtracted from the spectrum. (c) Parameter phase diagram predicted by the tight binding model, where we define the  $t_T = -0.38$ ,  $t_L = -0.68$ ,  $t_{K,A} = -0.02$ ,  $t_{K,R} = 0.1$ , and scan  $\Delta U_{3c}$  and  $U_{1a}$ . The central white regime corresponds to the fragile topological phase of the lattice. The parameter set in (a) falls into the topological phase after scaling, marked as a red circle.

a planar microcavity system consisting of etched microresonators, functioning as synthetic atoms in the lattice, similar to Refs. [41–43].

To map the proposed electromagnetic tight-binding model to this structure, we intentionally introduce an extended spacing to reduce (ideally to vanish) the overlapping of EM fields between each circular resonator, and subsequently only connect resonators at 1a and 3c sites to locally enhance couplings between them via links to increase the coupling contrast [Fig. 4(a)]. These links will consequently change the shape of resonators at 3c Wyckoff positions, hence inevitably affecting the on-site energy of azimuthal and radial modes. The elliptical aspect ratio of the resonators at 3c sites is tuned accordingly, whereas the shape of resonators at 1a Wyckoff positions are not changed since links connected to the 1a site will not break the degeneracy of two circularly polarized modes. The elliptical design does not break any crystalline symmetry of the space group and therefore the band representations previously introduced are still valid. The detailed geometric parameters and setup of numerical simulations are discussed in the Supplemental Material [29].

We numerically calculated the eigenfrequency spectrum of the structure and it was then fitted based on the tight binding model discussed in the previous section [red circles and blue lines in Fig. 4(b), respectively]. The fitting parameters for the numerical simulation results are  $t_L = -0.267$  meV,  $t_T = -0.149$  meV,  $t_{K,A} = -0.008$  meV,  $t_{K,R} = 0.039$  meV,  $t_{K,A} = 0.118$  meV,  $t_{K,A} = 0.00$  meV, and  $t_{K,A} = 0.00$  meV. Note that fitting parameters are now assigned with units to capture the actual energy scale in practice. In the current results, band representations and degeneracies are correctly captured. The numerical results indeed agree with the electromagnetic tight-binding model [Fig. 4(b)]. Four eigenmodes at the  $t_{K,A} = 0.00$  meV. We note that the direct imaging of symmetry representations at high-symmetry

points, together with the imaging of spectral flow at interface states of twisted boundary conditions, are two possible approaches to experimentally examine the topological nontriviality in these systems [25,44]. The upper band of the central four bands show flatness of  $\sim 1/10$  of the gap width near K and M points.

We further illustrate the calculated fragile topological phase diagram based on the tight-binding model in the parameter space [Fig. 4(c)], which can be helpful for further optimization of the structural design of a TFB microcavity array. Based on the fitting parameters of the simulation results in Fig. 4(a), we set  $t_T = -0.38$ ,  $t_L = -0.68$ , with finite Kagome coupling  $t_{K,A} = -0.02$ ,  $t_{K,R} = 0.1$ ,  $U_R = 0$ , and scanning  $\Delta U_{3c} = U_A - U_R$  and  $U_{1a}$  from -2 to 2. The topological phase is numerically characterized by two features: (1) the presence of two complete gaps between the central four bands with the upper and lower two bands; and (2)  $C_2$  eigenvalues at the M point of the central four bands are +1. The central region in Fig. 4(c) corresponds to the fragile topological phase, confirming our intuitive conjecture that a suppressed  $\Delta U_{3c}$ and  $U_{1a}$  will be beneficial for realizing fragile topological phases. Lastly, we discuss possible experimental realizations of our proposed designs. As we deduce from our previous calculation [Fig. 3(b)], the Kagome coupling is the most significant ingredient for enhanced band flatness. However, due to the non-negligible overlapping of electromagnetic modes in the microcavity array, it is challenging to selectively turn off the Kagome couplings. Additionally, for microcavity structures, the design of the reflectors directly affects the linewidth of the photonic bands, characterized by quality (Q-) factor. Consequently, in future study, the computer-assisted inverse design may be applied to further optimize the structure for lower Kagome couplings and enhanced Q-factor. In addition, for the condensation condition, we note that previous works have demonstrated that by controlling the excitation pattern, Bosonic condensation in higher bands is possible [38,45].

### V. CONCLUSION

In summary, we exploited the TQC theory to design a simple photonic lattice with fragile topological quasiflat bands, completely isolated from other trivial bands, manifesting its Wannier obstructed properties. We further proposed a microcavity array realization, where LT polarization splitting is taken into consideration, to host fragile quasiflat topological bands. A tight binding description and numerical simulations of the proposed microcavity system together demonstrate the validity of this topological lattice and can estimate the parametric requirement for future optimization and applications. Our designs are compatible with coupling the photonic cavity to excitonic materials to enable new experimental observations of the effect of quantum geometry and topology on polariton condensates [19,46].

### ACKNOWLEDGMENT

This work was supported by the Office of Naval Research via Grant No. N00014-22-1-2378.

- [1] S. Peotta and P. Törmä, Superfluidity in topologically nontrivial flat bands, Nat. Commun. 6, 8944 (2015).
- [2] Y. Cao, V. Fatemi, S. Fang, K. Watanabe, T. Taniguchi, E. Kaxiras, and P. Jarillo-Herrero, Unconventional superconductivity in magic-angle graphene superlattices, Nature (London) 556, 43 (2018).
- [3] V. Peri, Z.-D. Song, B. A. Bernevig, and S. D. Huber, Fragile topology and flat-band superconductivity in the strong-coupling regime, Phys. Rev. Lett. 126, 027002 (2021).
- [4] K.-E. Huhtinen, J. Herzog-Arbeitman, A. Chew, B. A. Bernevig, and P. Törmä, Revisiting flat band superconductivity: Dependence on minimal quantum metric and band touchings, Phys. Rev. B 106, 014518 (2022).
- [5] P. Törmä, S. Peotta, and B. A. Bernevig, Superconductivity, superfluidity and quantum geometry in twisted multilayer systems, Nat. Rev. Phys. 4, 528 (2022).
- [6] F. Xie, Z. Song, B. Lian, and B. A. Bernevig, Topology-bounded superfluid weight in twisted bilayer graphene, Phys. Rev. Lett. 124, 167002 (2020).
- [7] H. Tian, X. Gao, Y. Zhang, S. Che, T. Xu, P. Cheung, K. Watanabe, T. Taniguchi, M. Randeria, F. Zhang *et al.*, Evidence for Dirac flat band superconductivity enabled by quantum geometry, Nature (London) 614, 440 (2023).
- [8] H. C. Po, H. Watanabe, and A. Vishwanath, Fragile topology and Wannier obstructions, Phys. Rev. Lett. 121, 126402 (2018).
- [9] H. C. Po, A. Vishwanath, and H. Watanabe, Symmetry-based indicators of band topology in the 230 space groups, Nat. Commun. 8, 50 (2017).
- [10] B. Bradlyn, L. Elcoro, J. Cano, M. G. Vergniory, Z. Wang, C. Felser, M. I. Aroyo, and B. A. Bernevig, Topological quantum chemistry, Nature (London) 547, 298 (2017).
- [11] J. Kruthoff, J. de Boer, J. van Wezel, C. L. Kane, and R.-J. Slager, Topological classification of crystalline insulators through band structure combinatorics, Phys. Rev. X 7, 041069 (2017).
- [12] J. Cano, B. Bradlyn, Z. Wang, L. Elcoro, M. G. Vergniory, C. Felser, M. I. Aroyo, and B. A. Bernevig, Topology of disconnected elementary band representations, Phys. Rev. Lett. 120, 266401 (2018).
- [13] J. Zak, Band representations and symmetry types of bands in solids, Phys. Rev. B 23, 2824 (1981).
- [14] J. Zak, Band representations of space groups, Phys. Rev. B 26, 3010 (1982).
- [15] L. Michel and J. Zak, Connectivity of energy bands in crystals, Phys. Rev. B **59**, 5998 (1999).
- [16] I. Lukin, A. Sotnikov, and A. Kruchkov, Unconventional superfluidity and quantum geometry of topological bosons, arXiv:2307.08748.
- [17] A. Julku, G. M. Bruun, and P. Törmä, Excitations of a Bose-Einstein condensate and the quantum geometry of a flat band, Phys. Rev. B 104, 144507 (2021).
- [18] A. Julku, G. M. Bruun, and P. Törmä, Quantum geometry and flat band Bose-Einstein condensation, Phys. Rev. Lett. 127, 170404 (2021).
- [19] K.-E. Huhtinen, M. Dürrnagel, V. Peri, and S. Huber, Quantum geometry and the superfluid weight of a Bose-Einstein condensate, Bull. Am. Phys. Soc. (2024).
- [20] A. Kruchkov, Quantum geometry, flat Chern bands, and Wannier orbital quantization, Phys. Rev. B 105, L241102 (2022).

- [21] K. Sun, Z. Gu, H. Katsura, and S. Das Sarma, Nearly flatbands with nontrivial topology, Phys. Rev. Lett. 106, 236803 (2011).
- [22] E. Tang, J.-W. Mei, and X.-G. Wen, High-temperature fractional quantum Hall states, Phys. Rev. Lett. 106, 236802 (2011).
- [23] T. Neupert, L. Santos, C. Chamon, and C. Mudry, Fractional quantum Hall states at zero magnetic field, Phys. Rev. Lett. 106, 236804 (2011).
- [24] M. B. De Paz, M. G. Vergniory, D. Bercioux, A. García-Etxarri, and B. Bradlyn, Engineering fragile topology in photonic crystals: Topological quantum chemistry of light, Phys. Rev. Res. 1, 032005(R) (2019).
- [25] V. Peri, Z.-D. Song, M. Serra-Garcia, P. Engeler, R. Queiroz, X. Huang, W. Deng, Z. Liu, B. A. Bernevig, and S. D. Huber, Experimental characterization of fragile topology in an acoustic metamaterial, Science 367, 797 (2020).
- [26] B. Jiang, A. Bouhon, S.-Q. Wu, Z.-L. Kong, Z.-K. Lin, R.-J. Slager, and J.-H. Jiang, Observation of an acoustic topological euler insulator with meronic waves, Sci. Bull. 69, 1653 (2024).
- [27] D. Călugăru, A. Chew, L. Elcoro, Y. Xu, N. Regnault, Z.-D. Song, and B. A. Bernevig, General construction and topological classification of crystalline flat bands, Nat. Phys. 18, 185 (2022).
- [28] S. Xu, Y. Wang, and R. Agarwal, Absence of topological protection of the interface states in  $\mathbb{Z}_2$  photonic crystals, Phys. Rev. Lett. 131, 053802 (2023).
- [29] See Supplemental Material at http://link.aps.org/supplemental/ 10.1103/PhysRevB.110.045401 for the discussion of irreducible representations, the complete Hamiltonian of the microcavity system, and details of numerical simulations, which also includes Refs. [30–32].
- [30] M. I. Aroyo, J. M. Perez-Mato, C. Capillas, E. Kroumova, S. Ivantchev, G. Madariaga, A. Kirov, and H. Wondratschek, Bilbao crystallographic server: I. databases and crystallographic computing programs, Z. Kristallogr.-Cryst. Mater. 221, 15 (2006).
- [31] M. I. Aroyo, A. Kirov, C. Capillas, J. Perez-Mato, and H. Wondratschek, Bilbao crystallographic server. II. Representations of crystallographic point groups and space groups, Acta Crystallogr. A: Found. Crystallogr. 62, 115 (2006).
- [32] M. I. Aroyo, J. M. Perez-Mato, D. Orobengoa, E. Tasci, G. de la Flor, and A. Kirov, Crystallography online: Bilbao crystallographic server, Bulg. Chem. Commun. 43, 183 (2011).
- [33] T. Mizoguchi and Y. Hatsugai, Molecular-orbital representation of generic flat-band models, Europhys. Lett. 127, 47001 (2019).
- [34] T. Mizoguchi and Y. Hatsugai, Systematic construction of topological flat-band models by molecular-orbital representation, Phys. Rev. B **101**, 235125 (2020).
- [35] A. Alexandradinata, X. Dai, and B. A. Bernevig, Wilson-loop characterization of inversion-symmetric topological insulators, Phys. Rev. B **89**, 155114 (2014).
- [36] A. Bouhon, A. M. Black-Schaffer, and R.-J. Slager, Wilson loop approach to fragile topology of split elementary band representations and topological crystalline insulators with time-reversal symmetry, Phys. Rev. B **100**, 195135 (2019).
- [37] T. Byrnes, N. Y. Kim, and Y. Yamamoto, Exciton–polariton condensates, Nat. Phys. 10, 803 (2014).
- [38] F. Baboux, L. Ge, T. Jacqmin, M. Biondi, E. Galopin, A. Lemaître, L. Le Gratiet, I. Sagnes, S. Schmidt, H. E. Türeci,

- A. Amo, and J. Bloch, Bosonic condensation and disorder-induced localization in a flat band, Phys. Rev. Lett. **116**, 066402 (2016).
- [39] A. Amo, J. Lefrère, S. Pigeon, C. Adrados, C. Ciuti, I. Carusotto, R. Houdré, E. Giacobino, and A. Bramati, Superfluidity of polaritons in semiconductor microcavities, Nat. Phys. 5, 805 (2009).
- [40] M. Pieczarka, E. Estrecho, M. Boozarjmehr, O. Bleu, M. Steger, K. West, L. N. Pfeiffer, D. W. Snoke, J. Levinsen, M. M. Parish et al., Observation of quantum depletion in a non-equilibrium exciton-polariton condensate, Nat. Commun. 11, 429 (2020).
- [41] A. V. Nalitov, G. Malpuech, H. Terças, and D. D. Solnyshkov, Spin-orbit coupling and the optical spin Hall effect in photonic graphene, Phys. Rev. Lett. 114, 026803 (2015).

- [42] T. Jacqmin, I. Carusotto, I. Sagnes, M. Abbarchi, D. D. Solnyshkov, G. Malpuech, E. Galopin, A. Lemaître, J. Bloch, and A. Amo, Direct observation of Dirac cones and a flatband in a honeycomb lattice for polaritons, Phys. Rev. Lett. 112, 116402 (2014).
- [43] A. V. Nalitov, D. D. Solnyshkov, and G. Malpuech, Polariton ℤ topological insulator, Phys. Rev. Lett. **114**, 116401 (2015).
- [44] Z.-D. Song, L. Elcoro, and B. A. Bernevig, Twisted bulk-boundary correspondence of fragile topology, Science 367, 794 (2020).
- [45] L. Ge, A. Nersisyan, B. Oztop, and H. E. Tureci, Pattern formation and strong nonlinear interactions in exciton-polariton condensates, arXiv:1311.4847.
- [46] W. Liu, Z. Ji, Y. Wang, G. Modi, M. Hwang, B. Zheng, V. J. Sorger, A. Pan, and R. Agarwal, Generation of helical topological exciton-polaritons, Science **370**, 600 (2020).